Journal of Geoscience and Environment Protection, 2020, 8, 155-176
https://www.scirp.org/journal/gep
ISSN Online: 2327-4344
ISSN Print: 2327-4336

Pilot Test of the Permeable Reactive Barrier for Removing Uranium from the Flooded Gunnar Pit

Dexu Kong[1*], Lesley McGilp[1], Alexey Klyashtorin[1], Ian Wilson[1], Lee D. Wilson[2]

[1]Saskatchewan Research Council, 125-15 Innovation Boulevard, Saskatoon, Canada
[2]Department of Chemistry, University of Saskatchewan, 110 Science Place, Saskatoon, Canada
Email: *dexu.kong@src.sk.ca

How to cite this paper: Kong, D. X., McGilp, L., Klyashtorin, A., Wilson, I., & Wilson, L. D. (2020). Pilot Test of the Permeable Reactive Barrier for Removing Uranium from the Flooded Gunnar Pit. *Journal of Geoscience and Environment Protection, 8,* 155-176.
https://doi.org/10.4236/gep.2020.87009

Received: May 30, 2020
Accepted: July 26, 2020
Published: July 29, 2020

Abstract

This work reports on applying iron oxide coated sand (IOCS) media in an experimental permeable reactive barrier to remove uranium (U) species from uranium containing water. A field study was conducted at the legacy Gunnar uranium mine & mill site that was abandoned in the 1960s with limited to no decommissioning. The flooded Gunnar mine pit presently contains about 3.2 million m^3 of water contaminated by dissolved U (1.2 mg/L), Ra-226 (0.4 Bq/L), and minor concentrations of other contaminants (As, Se, etc.). The water is seeping over the pit rim into Lake Athabasca, posing potential environmental and health concerns. IOCS media can be used to immobilize uranium species through an adsorption process. Herein, the preparation of hydrous ferric oxide sorbents and their supported forms onto silica sands is described. Fourier transform infrared spectroscopy (FTIR) and powder X-ray diffraction (pXRD) were used for structural characterization. The adsorption properties of the IOCS sorbent media were modeled by the Langmuir adsorption isotherm, where a maximum uranium uptake capacity was estimated. Bench-scale adsorption kinetic experiments were also performed before moving to a field trial. Based on these lab results and input on field-scale parameters, a pilot permeable reactive barrier was fabricated and a field test conducted near the Gunnar pit in June 2019. This pilot test provided technical data and information needed for designing a full-scale permeable barrier that employs the IOCS media. This approach can be applied for *in-situ* water treatment at Gunnar and other legacy uranium sites.

Keywords

Adsorption, Breakthrough, Iron Oxide Coated Sand, Permeable Reactive Barrier, Uranium Species

1. Introduction

The abandoned Gunnar Mine and mill site are located at the northern shore of Lake Athabasca approximately 30 km southwest of Uranium city in northwestern Saskatchewan, Canada. The open pit mine was established in 1953 and operated through 1961. By that time, the pit was about 300 m long, 250 m wide, and up to 116 m deep, with a large opening to deeper mine areas. The operations on the site were ceased in 1964, because most of the available uranium ore had been extracted. Some decommissioning was carried out that focused mainly on equipment salvaging and capping of the mine shaft and openings. The pit with associated mine workings was flooded through blasting a narrow 50-m channel to Lake Athabasca. Upon flooding, the channel was backfilled with coarse waste rock material (Muldoon & Schramm, 2009). Due to improper decommissioning and multiple environmental issues associated with the remaining facilities, infrastructure, and contamination at the Gunnar mine site, the Saskatchewan Research Council (SRC) was retained to manage a remediation and cleanup project at the Gunnar site. The flooded pit at the Gunnar site now contains a total volume of approximately 3 million m^3 of water contaminated by dissolved uranium with a concentration of ~1000 μg/L. This is about two orders magnitude above the regulatory level set by the Saskatchewan Environmental Quality Guideline (SEQG). The water level in the pit is 1.5 to 2 m above that in Lake Athabasca, which allows some of the pit water to overflow annually through the backfilled channel into Lake Athabasca. Currently, a preferred mitigation option for the flooded pit is long-term monitoring of the water quality and surface flow. This approved option by the provincial and federal regulators cannot reduce current uranium loadings to Lake Athabasca. In principle, a permeable reactive barrier (PRB) technology can be applied to capture uranium from the pit water before it reaches the lake. In particular, iron oxide coated sands (IOCS) media can be utilized for the purpose.

The advantages of PRB technology relate to the lower cost of chemicals and energy consumption, where the PRB can function for decades with little maintenance required. Iron oxide minerals such as ferrihydrite and hematite are excellent adsorbents for adsorbing uranium species (Marshall et al., 2014). These iron oxide minerals can be prepared as nanoparticles with a high surface area, which favor their application as potential adsorbent materials. A complicating issue with the use of fine nanoparticle sorbents is their high mobility and recovery over multiple cycles of adsorption-desorption. Thus, it would be better to coat these iron oxide nanoparticles onto a silica sand substrate to immobilize them (Benjamin et al., 1996). IOCS media were prepared, and their uranium removal efficiency was tested at SRC labs. Several fix-bed filtration column tests were carried out to evaluate the feasibility of applying IOCS as a potential adsorbent media in the PRB. The test results from filtration columns were evaluated with breakthrough curve models such as the Adams-Bohart, Thomas, and Yoon-Nelson (Mahaninia & Wilson, 2017). The performance of a fixed-bed

column is described through the concept of the breakthrough curve. The shape of the breakthrough curve can yield important characteristics (the time for a breakthrough, the maximum adsorption capacity of the adsorption column), determining the optimum operation conditions of an adsorption column (Han, 2009). Based on the optimum operation conditions obtained from fix-bed filtration column tests, a pilot-scale PRB was designed in the 2019 winter period and shipped to the Gunnar mine site for later testing. **Figure 1(a)** shows the Gunnar mine pit before flooding with the Lake water (Muldoon et al., 2013), and **Figure 1(b)** shows the field test location of the pilot PRB. The northeast corner of the Gunnar pit was chosen as the field test location because this relatively shallow area can be sheltered from the winds, and it can provide ideal conditions for safe installation and maintenance, as well as favorable conditions for consistent water sampling during the test period.

There are three goals of this study: 1) To test whether IOCS media can immobilize uranium species via surface adsorption; 2) To generate data for the pilot-scale permeable reactive barrier through lab-scale column adsorption tests with uranium containing water; and 3) To test whether the uranium removal efficiency can be scaled-up successfully for the pilot-scale permeable reactive barrier field test at the Gunnar pit site. The preparation and characterization of IOCS are described herein, along with the uranium uptake by IOCS media in static batch and dynamic column adsorption experiments.

2. Experimental

2.1. Materials and Equipment

Silica sands were purchased from the Lane Mountain Company with different particle size distribution (LM 70 and LM 125 sands). Ferric nitrate nonahydrate, sodium bicarbonate, sodium carbonate, nitric acid, and monopotassium phosphate (H_2KPO_4) were purchased from Fisher Scientific Canada. All chemicals were ACS grade and used as received.

The lab scale test equipment includes glass beakers, overhead stirrers, a pH meter, timers, a 9 cu. ft. concrete mixer, 20 L pails, a moisture analyzer, an oven, a conductivity meter, and a constant head permeameter to measure the permeability

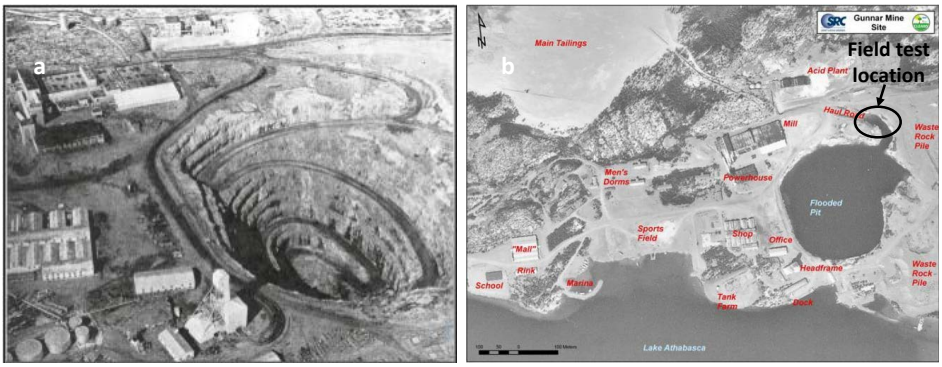

Figure 1. (a) Gunnar mine pit before flooding, and (b) field test location.

of IOCS. For the field test, equipment includes a pilot permeable reactive barrier (PRB) with 132 cm × 59.4 cm × 94.6 cm (L × W × H) in dimension, the pilot PRB has 2 inches diameter opening for the inlet and outlet ports. Inside this pilot PRB, there is a perforated plate and a 45 μm stainless steel fine mesh to contain the sand particles. A 1/2 HP submersible pump was used to deliver water from the Gunnar pit to go through the PRB box. A gas generator was used to power the submersible pump.

2.2. Methods of Synthesis of Iron Oxide and IOCS

2.2.1. Synthesis of a Ferrihydrite Mineral

The sodium bicarbonate solution was made by dissolving 4.84 g of Na_2CO_3 in 20 g deionized (DI) water. The ferric nitrate solution was made by mixing 10.76 g of $Fe(NO_3)_3 \cdot 9H_2O$ in a 250 mL beaker with 20 g of DI water. Once the solution was homogenized, the ferric nitrate solution was added into the sodium bicarbonate solution to precipitate the ferrihydrite minerals. The pH of the final slurry was monitored, where it was set to ca. pH 6.8 or by adjusting the pH with some dilute aqueous HNO_3 to obtain a neutralized slurry.

2.2.2. Lab-Scale of Synthesis Iron Oxide Coated Sands

In a 250 mL beaker, about 2.42 g of Na_2CO_3 was dissolved in 10 g of DI water. The chemicals were mixed at low speed about 40 rpm, otherwise too much CO_2 is trapped from the air. The above solution was added into the 400 mL beaker with the sand, and then hand mixed for 5 mins with a glass rod or a spatula. A separate ferric nitrate solution was prepared by dissolving 5.38 g of $Fe(NO_3)_3 \cdot 9H_2O$ in a 250 mL beaker with 10 g of DI water. The above solution was added into the 400 mL beaker with sand, where it was hand mixed for 5 mins with a glass rod or a spatula. Using a pH meter to check the final pH of the mixture (pH ~ 6).

2.2.3. Method of Large-Scale Synthesis of Iron Oxide Coated Sand with a Cement Mixer (70 kg per Batch)

1. Preparation of chemicals

0.656 M ferric nitrate nonahydrate solution (10 L) was prepared using 2575.8 g of ferric nitrate nonahydrate was dissolved in 10 L water. To make 10 L of 1.14 M sodium carbonate chemicals, 1176.12 g of sodium carbonate was dissolved into 10 L water.

2. Coating silica sands with iron oxide chemicals

Each bag of the LM 125 sand is 22.68 kg, three bags of sand were added one by one into the cement mixer. One bag of the LM 125 sand was poured into the concrete mixer while the cement mixer was running. About one-third portion of the 10 L sodium carbonate chemicals were added in the cement mixer, where the setup for the production of the IOCS material is shown in **Figure 2**. Repeating the sand and sodium carbonate addition for two more times until 68.04 kg of the sand and sodium carbonate chemicals were added. Mixing the sodium carbonate solution with the LM 125 sand for 8 mins, and then slow addition of all the 10 L ferric nitrate nonahydrate solution into the concrete mixer with mixing for

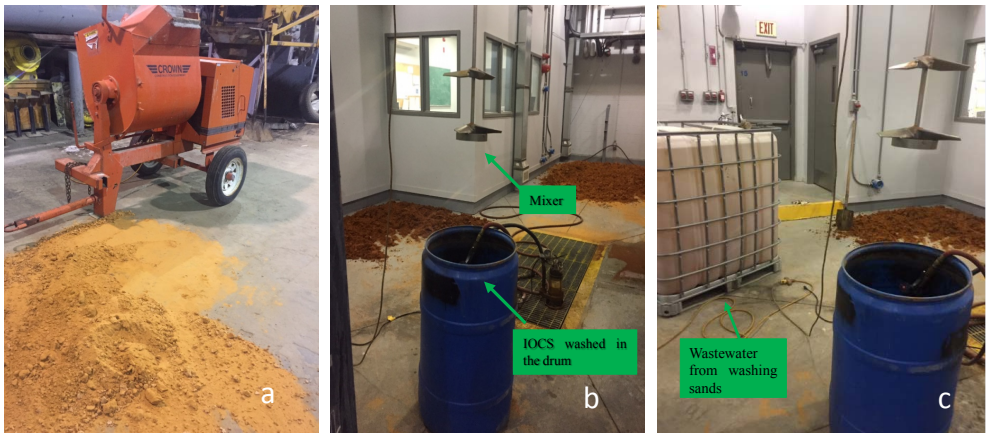

Figure 2. (a) The IOCS on the floor made by the cement mixer, (b) the mixer and drums used to the wash coated IOCS, (c) and the wastewater produced from the IOCS washing process.

another 8 mins. Once all of the silica sands turn to yellow-reddish color, the coated sand was poured out and spread onto the floor to dry under ambient room temperature conditions. Upon drying of the coated sands, the product was washed by tap water to remove residual chemicals from the coated sands, where washing continued until the conductivity (ca. 10 mS/m) for the supernatant and the washing water was the same. At the end of the sand coating process, the wastewater generated from the coating process was tested for its iron content. The iron content of the wastewater was below the regulatory limit set by the City of Saskatoon, where it was safely discharged back into the municipal sewer system.

2.3. Characterization of Iron Oxide Chemicals and Coated Sands

2.3.1. The pH for the Point of Zero Charge (pH_{pzc})

The method used to determine the point of zero charge of sorbents was adopted from a previously reported study (Udoetok et al., 2016). In brief, 20 mL of 0.01 M NaCl solution was transferred into each of nine glass vials (7 dram). The pH of the respective solutions was adjusted by NaOH/HCl to obtain the following pH ranging from 2.0 to 13.0. Approximately 0.5 g of sorbent material was added to each solution and the mixtures were equilibrated for 48 h before the final pH was measured. A plot of the final pH versus initial pH was plotted, where the intersection point was recorded as the pH for the point of zero charge (pH_{pzc}) for each sorbent.

2.3.2. pXRD Analysis

Powder X-ray diffraction (pXRD) was used to observe the long-range order of the ferrihydrite compound and the IOCS material. The pXRD instrument (Model: Empyrean, manufacturer: PANalytical, The Netherlands) fitted with Co K-alpha (λ = 1.79 Å) X-ray irradiation source. The pXRD results were compared to the simulated spectra from the X'pert Highscore Plus software (Ver. 3.0b (3.0.2), Panalytical, Almelo, the Netherlands).

2.3.3. FTIR Analysis

Fourier Transform infrared (FTIR) spectra of the materials were obtained with a Bio-Rad FTS-40 spectrophotometer, where samples were diluted with KBr (FTIR grade, Alfa Aesar) at 10% by weight and 256 scans from 4000 to 400 cm^{-1} with a spectral resolution of 4 cm^{-1}.

2.3.4. TEM Imaging

Transmission electron microscopy (TEM) images were obtained using a Hitachi HT-7700 microscope with a 100 kV voltage. Samples were prepared by dispersing into ethanol solution with a sonication bath, then a drop of the sample in ethanol was deposited onto a carbon-coated copper TEM grid without staining agent. The samples were examined at variable scales (50 nm, 100 nm, and 200 nm).

2.4. Adsorption Tests

2.4.1. Uranium Adsorption Batch Tests at Equilibrium

An equilibrium adsorption study of uranium uptake at 295 K was conducted in batch mode with accurately known amounts of adsorbent (ca. 0.6 g). Each adsorbent was dispensed into 5 dram glass vials containing 15 mL uranium solution at pH 8.2 and initial concentration (100 ppb to 1000 ppb) values. The samples were placed on a shaker table at a constant speed (250 rpm) at 295 K for 24 h. After attaining equilibrium, 0.5 mL of each sample was withdrawn and centrifuged. 300 μL of the supernatant solution was isolated after centrifuging with subsequent dilution of 2.70 mL of the monopotassium phosphate buffer (3.5% (v/v) of 70 wt.% HNO_3 solution in 1 M H_2KPO_4) to enable laser induced phosphorescence analysis of uranium over a linear calibration range (Jung et al., 1987, Sheng & Fein, 2014). Triplicate measurements were made to obtain average estimates of uptake, according to the calibration curve. Two adsorption models (Langmuir and Freundlich) were used to analyze the adsorption isotherm results by a non-linear fitting routine. The Langmuir model assumes monolayer adsorption with a finite number of homogeneously distributed binding sites over the adsorbent surface, where no interaction occurs between adsorbed species. Equation (1) describes the Langmuir model:

$$q_e = \frac{q_m K_L C_e}{\left(1 + K_L C_e\right)} \tag{1}$$

In Equation (1), q_m is the maximum amount of the adsorbate bound as a monolayer onto the adsorbent, q_e is the amount of the adsorbate bound at equilibrium, C_e is the unbound adsorbate concentration in solution at equilibrium, and K_L is the Langmuir adsorption constant. The empirical Freundlich model is very similar to the Langmuir model except that it assumes the sorbent has a heterogeneous surface with binding sites that are inequivalent with variable binding affinity. Equation (2) describes the Freundlich model:

$$q_e = K_f C_e^{\frac{1}{n}} \tag{2}$$

In Equation (2), q_e is the amount of the adsorbate bound onto the adsorbent at equilibrium, while K_f and n are Freundlich adsorption constants for a given adsorbate and adsorbent at a particular temperature. The best-fit between the calculated and experimental data with each isotherm model was obtained by minimizing the sum of squares of errors (SSE), respectively.

2.4.2. Uranium Adsorption Kinetics at Variable Temperature

The kinetic uptake of uranium from aqueous solution was carried out in a 300 mL beaker with a thermal jacket, where ca. 4 g of IOCS was added into 200 mL of uranium solution (1 ppm). The adsorption kinetics was studied over a 90 min interval, 0.50 L of the sample were taken at different time intervals, where a 300 μL aliquot was isolated and subsequently diluted with 2.70 mL of the monopotassium phosphate buffer (3.5% (v/v) of 70 wt.% HNO_3 solution in 1 M H_2KPO_4) prior to absorbance measurements. The uranium uptake by the various adsorbent systems was analyzed using Equation (3) and Equation (4). Both pseudo-first-order (PFO) and pseudo-second-order (PSO) models were used to process the adsorption kinetics isotherm data for the uranium removal by IOCS. The PFO kinetic model assumes there are a large number of available adsorption sites for uranium uptake. Equation (3) is a non-linear equation describing the PFO kinetics model:

$$q_t = q_e\left(1 - e^{-k_1 t}\right) \tag{3}$$

q_e and q_t are the amounts of uranium adsorbed (mg/kg) at steady state and variable time (t; min) by the adsorbent. The PFO rate constant (k_1) was determined from a non-linear fit by minimization of the SSE for plots of q_t against time (t). The experimental value of q_e for the uranium adsorbed (mmol/g) at steady state conditions can be calculated from the PSO model, according to Equation (4).

$$q_t = \frac{k_2 q_e^2 t}{\left(1 + k_2 q_e t\right)} \tag{4}$$

The PSO rate constant k_2 is determined from a non-linear fit, while other parameters are defined above. The value of SSE was minimized for q_t against time. The temperature can affect the uranium adsorption rate by the iron oxide coated sands, where kinetic adsorption experiments were studied at variable temperatures (5˚C, 15˚C, and 25˚C).

2.5. pH Effect on the Uranium Uptake by IOCS

Since the adsorption process of uranyl carbonate anions onto IOCS sorbent media is based on an electrostatic mode of interaction, the surface charge of the IOCS will impact the adsorption capacity of the uranyl carbonate anion. The pH of the uranium containing water can affect the surface charge of the IOCS greatly. IOCS adsorbents (ca. 0.5 g) were placed into each 4 oz. glass jars with 100 mL of variable pH (6.5, 7, 7.5, 8, and 8.5). These samples were placed on a shaker to mix at 120 rpm overnight to achieve equilibrium. The uranium concentration of

the aqueous phase for each sample was analyzed to estimate the level of adsorbed uranium ions by IOCS.

2.6. Sand Permeability Tests

To design the filtration column with optimal height to apply the pressure on top of the IOCS filter bed, it is important to estimate the permeability of the IOCS column bed media. Darcy's law is used to determine the permeability of the IOCS column, which is described by Equation (5). The goal of the IOCS permeability test is to estimate the value of the permeability coefficient (K).

$$Q = K\frac{-\Delta PA}{\mu L} \tag{5}$$

The flow rate is denoted as Q (m^3/s). The pressure change (ΔP) can be obtained by calculating the depth of the water on top of the IOCS filter bed, and the cross-sectional area (A) of the IOCS filter bed can be calculated with the inner diameter of the fix bed column. The water viscosity (μ) is used here and the length (L) of IOCS bed is the same as the height of the IOCS filter bed. Three IOCS permeability tests were conducted at room temperature and ambient pressure. The same fixed-bed column and flow rates were used for those tests, but each test had a different height of the IOCS bed. Three IOCS permeability values were obtained and then compared.

2.7. Lab-Scale Column Breakthrough Tests

IOCS (ca. 30 g) was loaded into a lab-scale filtration column with a diameter of 2.54 cm and 14 cm in height to produce the uranium breakthrough curve for the IOCS media. Glass wool was used at the inlet of the fixed bed column to prevent loss of media. A precision digital peristaltic pump was used to deliver the uranium containing water to flow through the IOCS column media. The effects of the depth-to-width ratio and flow rate of the filtration column were studied with the filtration column at a fixed diameter, and various amounts of IOCS were added to alter the depth of the adsorption bed. Three depth-to-width ratios were studied (1.14, 2.21, and 4.43). The mathematical models used in this work are summarized in Table 1, model parameters and related equations of the non-linear model are listed. Experimental data were processed by non-linear fitting methods to compare the accuracy and evaluate the errors of the experimental data.

Table 1. Adsorption models for the breakthrough curves.

	Non−linear form of the breakthrough curve
Adams-Bohart model	$\frac{C_t}{C_o} = \exp\left(K_{ab}C_o t - K_{ab}N_o\frac{H}{v}\right)$
Thomas model	$\frac{C_t}{C_o} = \frac{1}{1+\exp\left(\frac{K_{th}q_e m}{Q} - K_{th}C_o t\right)}$

The Adams-Bohart and Thomas models have been employed to describe dynamic adsorption in columns based on the shape of the breakthrough curves. Herein, the breakthrough curves of a fixed-bed column were fitted non-linearly by plotting C_t/C_o against t, where column parameters were estimated for values of N_o (kg/L) column adsorption capacity, q_e (mg/kg) the adsorption capacity of the media, K_{ab} Adams-Bohart constant and K_{th} Thomas constant. Although both methods are generally used to study the influence of the flow rate, initial solute concentration, and the depth-to-width ratio of the fixed-bed column. The Adams-Bohart model is generally used to study the effect of the initial solute concentration and the depth-to-width ratio of the column. The N_o value allows for a prediction of the column bed performance from the initial solute concentration. The value of K_{ab} represents the rate of phase transfer of the adsorbate from the liquid phase to the sorbent phase, where K_{ab} can be used to predict the optimal bed height. A large value of K_{ab} relates to a delayed breakthrough time, while a lower value of K_{ab} indicates that a longer column bed is required to offset rapid breakthrough (Mahaninia & Wilson, 2017). The Thomas model is used to study the effects of the flow rate on the performance of the fixed-bed column. The value of q_e represents the adsorption capacity of the media in the fixed-bed column, and the large q_e is favorable in optimizing the column performance. The Thomas model is suitable for adsorption processes where the external and internal diffusion are not the limiting steps (Mahaninia & Wilson, 2017). To study the flow rate effect on the uranium removal of the filtration column, the same amount of IOCS adsorbents (30 g) was tested at different flow rates to see the changes in uranium removal efficiency.

2.8. Pilot-Scale PRB Breakthrough Tests

The pilot PRB was fabricated to hold 600 kg IOCS for treating uranium containing water in the Gunnar pit. **Figure 3** shows the configuration of the pilot PRB equipment.

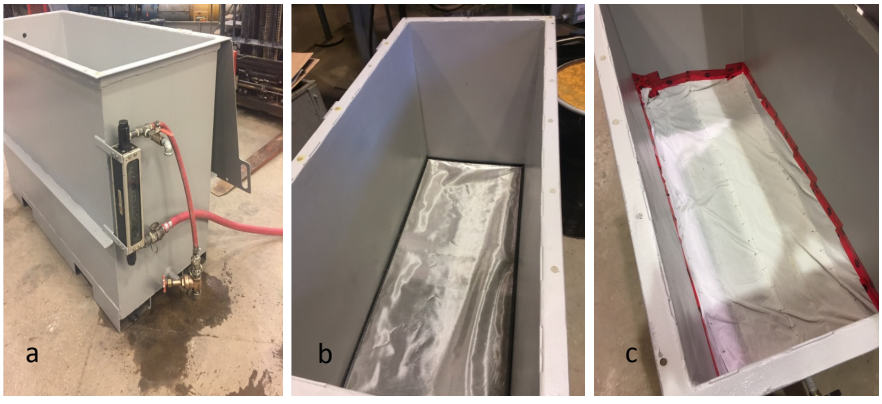

Figure 3. Illustration of the PRB equipment setup: (a) outside view of the pilot PRB with the flow meter, valves and hoses connected; (b) the perforated plate supported 75 μm fine mesh with the screen inside the pilot PRB box; and (c) the filter socks used on the top of the fine mesh screen to prevent loss of the IOCS to the bottom of the PRB box.

During the winter 2019 period, the pilot PRB unit and IOCS were shipped to the Gunnar mine site for the field tests. The PRB was positioned on the north-east corner of the Gunnar pit, and the IOCS media (ca. 600 kg) was loaded into the PRB. A 1 HP submersible pump was placed at about 6 m depth and 50 m away from the shore of the Gunnar pit to carry the uranium containing water from the Gunnar pit to the pilot PRB. A flow meter was used to monitor the flow rate of the incoming water. The flow rate at the outlet was also double checked with a graduated cylinder and a stopwatch. The performance of the pilot PRB was evaluated by sampling the water from both the inlet and outlet at different time intervals. The samples were preserved by adding nitric acid and sent to the Saskatchewan Research Council environmental analytical lab for uranium level analysis (**Figure 4**).

3. Results & Discussion

3.1. The pH for the Point of Zero Charge (pH_{pzc})

The pH of the solution can affect the surface charge of adsorbents, where the pH of point of zero charge (pH_{pzc}) is the pH where the net surface charge of the material is zero (Hubbe et al., 2012). One of the adsorption mechanisms is through electrostatic interactions between the adsorbent and charged adsorbate ions. The net charge of the adsorbent in the solution can be negative if the solution pH is greater than the pH_{pzc}. This relates to the adsorption of OH^- and/or the dissociation of H^+ at the base sites of the adsorbent surface. In cases where the solution pH is below the pH_{pzc} value, the adsorbent surface becomes positively charged due to the association of H^+ onto the adsorbent surface. The results obtained herein show that the pH_{pzc} of the IOCS materials is ca. 7.8 while that of silica sand is near 6.5 (cf. **Figure 5(a)**, **Figure 5(b)**). The pH_{pzc} value for the silica sand from this work is similar to other independent studies, where granite sands have a slightly lower pH_{pzc} at 6.2 (Khan & Sarwar, 2007). The similar values of pH_{pzc} for the IOCS is evidenced by the following comparison, where the pH_{pzc} (hematite/silica composite) is 7.8 (Rusch et al., 2010).

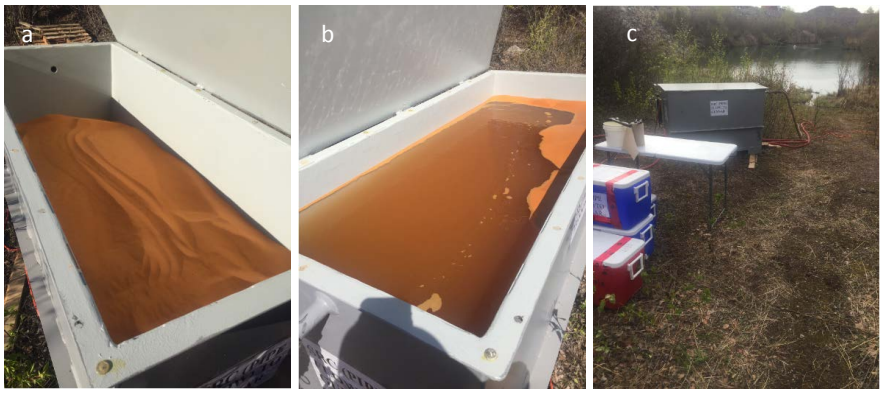

Figure 4. Pilot PRB filled with IOCS adsorbents: (a) before pit water addition; (b) after the pit water was pumped through the pilot PRB; and (c) overall setup of the pilot PRB near the Gunnar pit.

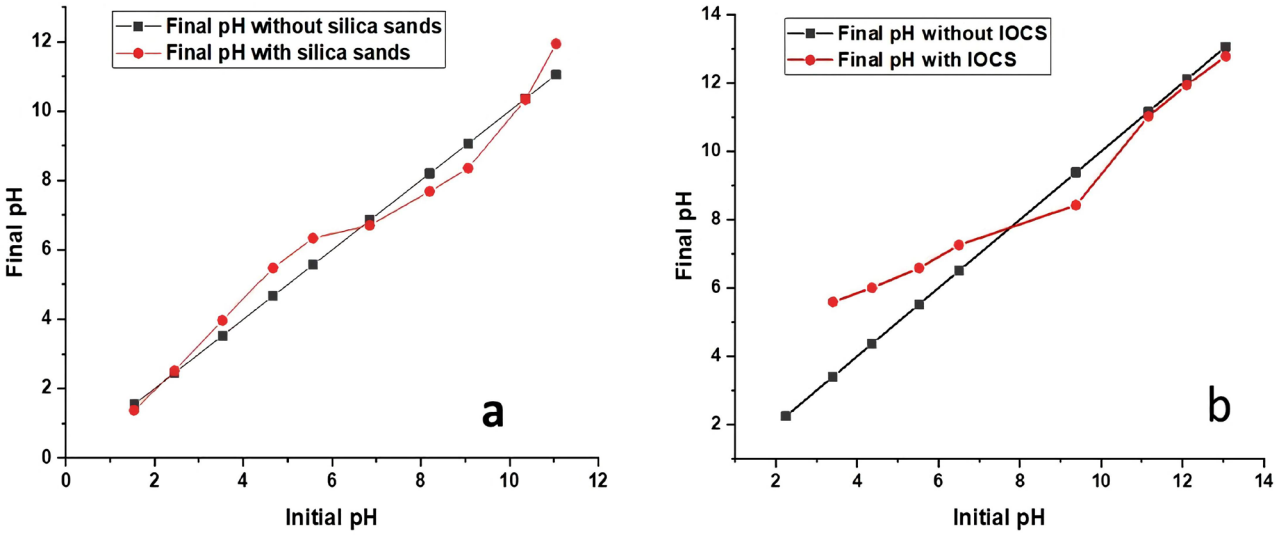

Figure 5. pH at the point of zero charge determination: (a) silica sands; and (b) IOCS media.

3.2. pXRD Results

The pXRD results confirm the ferrihydrite was successfully prepared, and the ferrihydrite minerals were transformed to hematite (a more stable form of iron oxides) upon drying. The ferrihydrite spectra is a typical two-line ferrihydrite (Schwertmann & Cornell, 2000), as shown in **Figure 6**, where two broad lines support the amorphous structure of such ferrihydrite minerals. The sharp and more intense hematite pXRD lines indicate that hematite has a more ordered and crystalline structure, as compared with ferrihydrite. A comparison of the XRD spectra from IOCS, silica sands with hematite, and ferrihydrite reveal that there were no obvious signatures of ferrihydrite and hematite in the IOCS spectra. Most of the silica sand signatures were evident in the IOCS pXRD spectra as less intense and broader lines. The reduced and broadened silica sand features in the IOCS pXRD results indicated that the iron oxide minerals were efficiently coated overall, and the crystalline nature of the silica sand was altered upon coating with these iron oxide minerals.

3.3. FTIR Spectral Results

FTIR spectra were obtained to evaluate the role of active functional groups that form bonds between the iron oxides and the silica sand supports (**Figure 7**). The IR bands at 1572 cm^{-1} relate to Fe-O of the ferrihydrite and hematite minerals. A broad IR band near 3327 cm^{-1} relates to the OH stretching of the hydrous ferric oxide (ferrihydrite) (Schwertmann & Cornell, 2000). The reduced OH signature from the IOCS with 12% Fe content to IOCS with 0.5% Fe content indicated the OH groups from the iron oxide minerals are interacting with the silica sand substrate. The size of the OH peaks also indicates that the amount of the iron oxides can be coated onto the silica sand was limited, where the IOCS target to have a 12% iron content was not met. The IOCS material was estimated to have a similar content to the iron oxide signature for the IOCS material with a

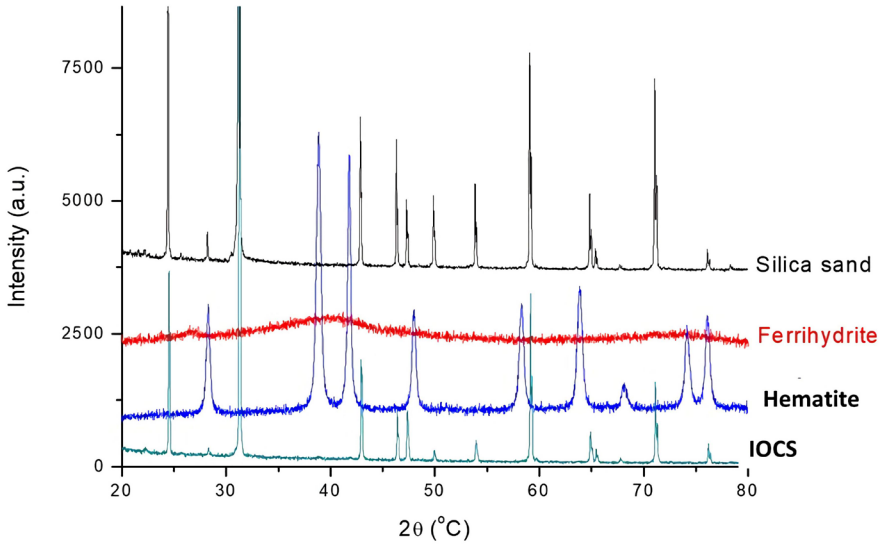

Figure 6. pXRD profiles of ferrihydrite, hematite, silica sands, and IOCS.

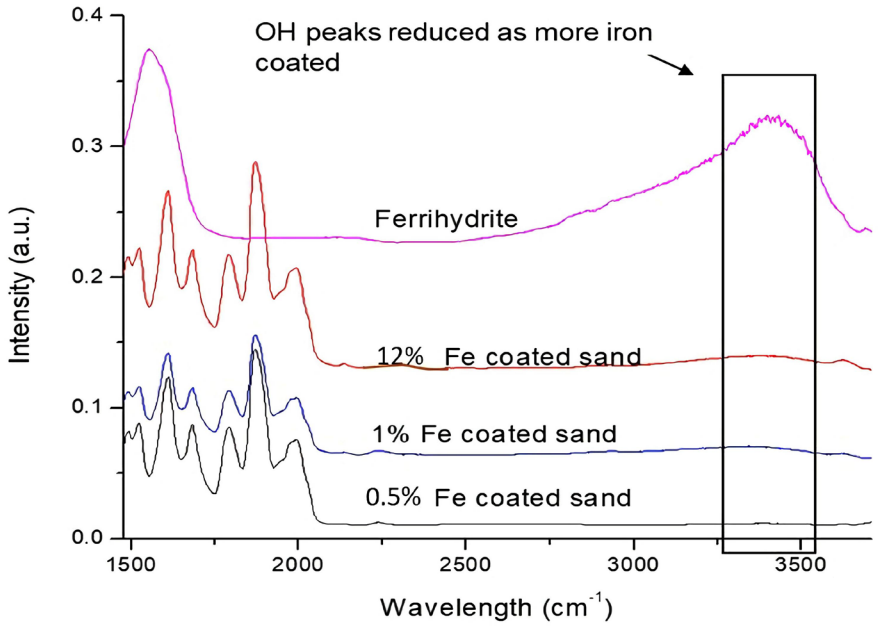

Figure 7. FTIR results of IOCS prepared with different loading levels of iron (%).

1% iron content. The FTIR results indicated that the amount of iron oxide that can be coated onto the silica sands was limited, where a 12% iron content loading of IOCS was not achieved by the sand coating process described herein. The actual amount of IOCS can be coated was also confirmed by the iron content analysis. The optimum Fe coating efficiency was found for IOCS made by targeting a 0.5% iron content.

3.4. TEM Imaging Results of Ferrihydrite Minerals and the IOCS

Figure 8 shows TEM images of synthesized ferrihydrite nanoparticles, where these nanoparticles were approximately sphere-shaped with large cluster aggregates. A

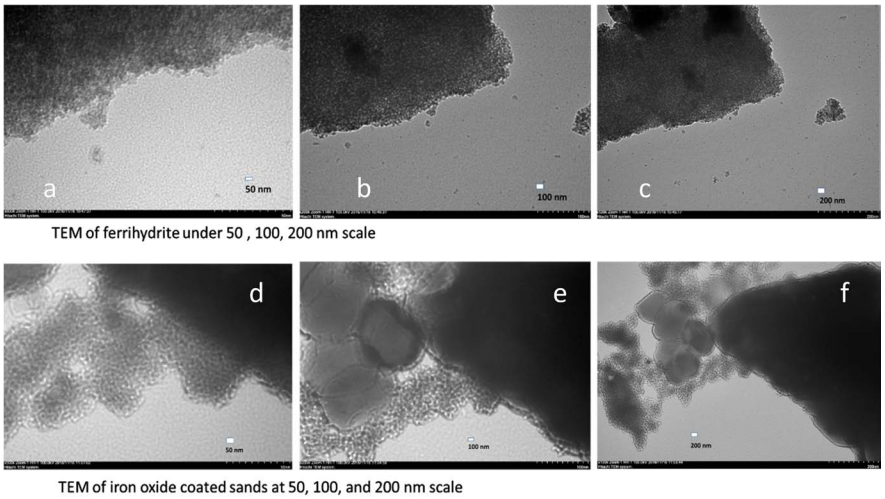

Figure 8. TEM images of the ferrihydrite and IOCS materials.

comparison of these images with literature results reveals that the morphology of these ferrihydrites was in agreement reported in Schwertmann's study (Schwertmann & Cornell, 2000). Hence the formation of ferrihydrite nanoparticles was confirmed herein. **Figures 8(d)-(f)** are the IOCS TEM images, where the dark region on the right side of those images was part of the silica sand particles. In the TEM image (cf. **Figure 8(f)**), there is evidence of iron oxides bonded to the silica sand, where these iron oxides resemble a mixture of ferrihydrite and hematite. The hematite nanoparticles might result from the transformation of those ferrihydrites during the drying process (Cornell & Schwertmann, 2003). A similar observation was noted for the TEM image in **Figure 8(e)**, where a mixture of ferrihydrite and hematite minerals was observed on the silica sand surface. For the TEM image in **Figure 8(d)**, the silica sand was covered by dispersed ferrihydrite. Comparison of **Figure 8(d)** and **Figure 8(a)** reveals that **Figure 8(d)** indicated greater dispersal of ferrihydrite nanoparticles onto silica aids the dispersal of the iron oxide, in agreement with the use of silica to promote ferrihydrite nanoparticle formation described elsewhere (Xiong & Peng, 2008).

3.5. Factors Affecting Uranium Uptake

3.5.1. Effects of Solid-to-Liquid Ratio and Uranium Feed Concentration on the Adsorption Tests

The experimental data was fitted well by the Langmuir isotherm model. The maximum adsorption (q_m) capacity of the IOCS was about 555 μg/g at pH 8 with a 0.1% solid-to-liquid ratio. The R^2-value was 0.969, as revealed by the goodness of fit between the model and experimental data in **Figure 9**. The adsorption capacity of the IOCS adsorbent dropped dramatically with an increase in the solution pH. **Table 2** shows that the solid-to-liquid ratio can affect the adsorption capacity of IOCS, where a lower solid-to-liquid ratio yields a greater adsorption capacity for IOCS. Even at the fixed adsorbate concentration, the chemical potential of the adsorbate is altered with changes in the fractional level of the adsorbate in

Table 2. Adsorption parameters obtained according to the Langmuir model.

Equation	$q_e = q_m * K * C_e / (1 + K * C_e)$	Value	Adj. R-Square
0.1% solid to liquid ratio	K	0.00297	0.969
	q_m	555	
2% solid to liquid ratio	K	0.00288	0.978
	q_m	32.6	
4% solid to liquid ratio	K	0.00428	0.973
	q_m	10.4	

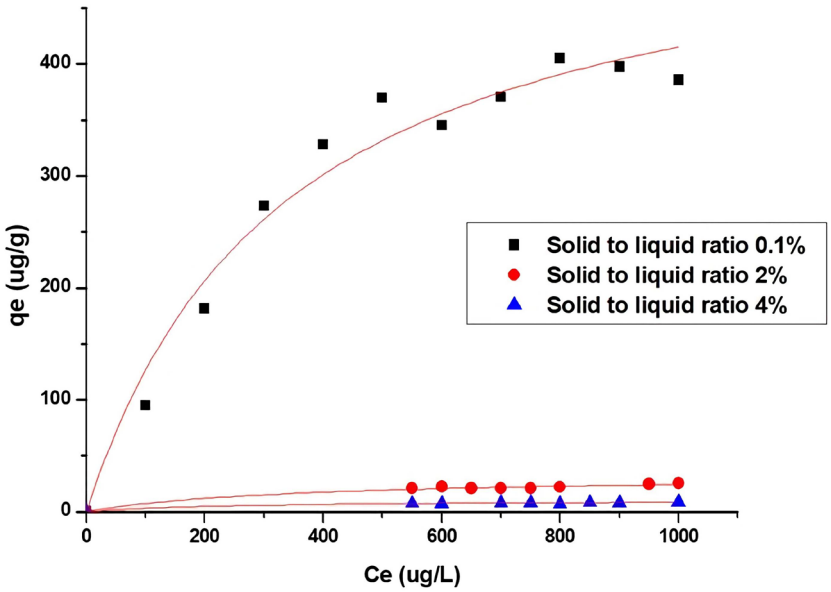

Figure 9. Isotherm profile of the uranium uptake by IOCS.

the whole solid-liquid system. The changes in the chemical potential of the adsorbate also affect the adsorption capacity of the adsorbent at its equilibrium state. The adsorption capacity of the adsorbent is known to vary upon changes to the solid-to-liquid ratio on the grounds of a greater equilibrium driving force as the level of adsorbate increases relative to the solid phase adsorbent. As well, the occurrence of potential aggregation of the adsorbents may occur at variable solid-to-liquid ratios, where aggregation may reduce the effective adsorbent surface area during the adsorption process.

In Table 2, "q_m" (μg/g) is the maximum adsorption capacity of the IOCS adsorbent, "K" (L/μg) is the Langmuir constant, "C_e" (μg/L) is the concentration of the adsorbate (uranium species in this case) at the equilibrium state. "q_e" (μg/g) is the uranium species adsorption capacity of the adsorbent IOCS.

3.5.2. Uranium Adsorption Kinetics and Variable Temperature Study

Adsorption kinetics experiments were studied at three different temperatures, where the pseudo second order rate model was used to evaluate the kinetic isotherm profiles. In Figure 10, the adsorption at 25˚C showed the highest uptake.

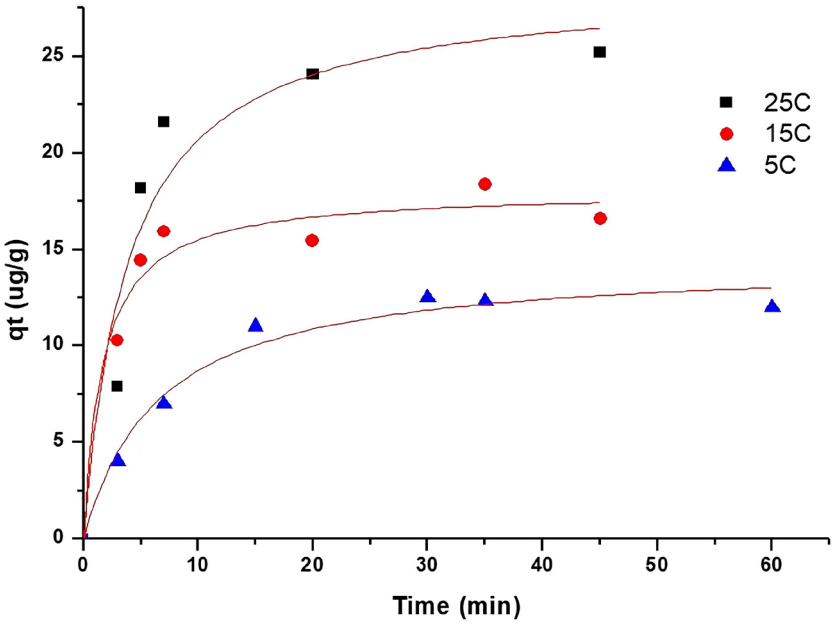

Figure 10. The pseudo second order model fitting to the experimental data at variable temperature.

As the temperature decreased, the uranium uptake by the IOCS adsorbents also decreased, indicative of an exothermic adsorption process. Comparing the slopes of three profiles in Figure 10 indicates that the fastest adsorption rate occurred between 15˚C to 25˚C, where the most rapid adsorption occurs within the first 10 mins of the process.

In Table 3, the low uranium uptake values resulted from the high pH (8.4) values employed at that condition.

3.6 pH Effects on the IOCS Uranium Uptake

The surface charge of IOCS can influence the amount of uranyl carbonate anions ($UO_2(CO_3)_3^{4-}$) that can be adsorbed (Sherman et al., 2008; Markich, 2002). The pH of the uranium containing water can also affect the surface charge of IOCS. Thus, a pH study of the IOCS adsorption process was carried out to determine the optimal pH value and the amount of uranyl carbonate anions that can be immobilized by IOCS. According to Table 4, the amount of uranium immobilized by IOCS decreased as the pH increased. A comparison of the q_e values of IOCS at pH 7 and pH 8.5 indicate that the uranium adsorption capacity of IOCS increases by a factor of 5 in response to the pH decrease from 8.5 to 7.

The term "C_o" is the original concentration of the adsorbate (uranium species) in the waste water, "C_e" is the concentration of the adsorbate at the equilibrium state, "V" is the volume of the waste water, "Wt." is the weight of the IOCS adsorbent used, and the term "q_e" (μg/g) is the uranium species adsorption capacity of the IOCS at equilibrium. The date in Table 4 reveal a reduction in uranium uptake as the pH of the uranium waste water increases. Comparing the q_e values of IOCS at pH and 7 and pH 8.5, we concluded the uranium adsorption capacity of

Table 3. The pseudo second order model parameters from the kinetic adsorption study at variable temperature.

Temp.	$q_t = \left(k * q_e^2 * t\right) / \left(1 + k * q_e * t\right)$	Value	Adj. R^2
25˚C	k	0.00891	0.909
	q_e	28.8	
15˚C	k	0.0332	0.960
	q_e	18.1	
5˚C	k	0.0105	0.976
	q_e	14.5	

Table 4. The effects of pH on the IOCS adsorption properties with uranyl carbonate.

pH	C_o (μg/L)	C_e (μg/L)	Wt. (g)	V (L)	q_e (μg/g)
6.40	980	29	0.503	0.0999	189
7.27	980	181	0.497	0.100	161
7.33	980	326	0.500	0.0999	131
7.89	980	612	0.499	0.100	73.8
8.30	980	704	0.503	0.101	55.1
8.63	980	816	0.507	0.0100	32.4

the IOCS can increase 5-foldby changing the pH of the uranium wastewater from 8.5 to 7.

3.7. Sand Permeability Tests

To optimize the IOCS permeability for the field pilot PRB test, three portions of the IOCS were prepared using LM 125 sands that were mixed with one portion of the IOCS made from LM 70 sands. The hydraulic conductivity (K) of the mixed IOCS was measured as 3.85×10^{-3} cm/S. The permeability parameter was used to design IOCS bed height and calculate the pumping power needed to conduct the field test at the Gunnar pit site.

3.8. Lab-Scale Column Breakthrough Tests

The breakthrough curve results were fit using the non-Linear forms of the Adams-Bohart and Thomas models, as illustrated below. **Figure 11(a)** shows the effects of the depth-to-width ratio of the column to the uranium level in the effluent. **Figure 11(b)** shows the effects of the flow rate of the column to the uranium level in the effluent.

In **Figure 11(a)**, the Adams-Bohart model was fitted to the breakthrough curve results that showed that the uranium adsorption capacity of the column (N_o) decreases as the bed depth (or D/W ratio denotes the depth-to-width ratio) increases. The trend was consistent with the results reported by Han's group (Han, 2009). In **Figure 11(b)**, the Thomas model was fitted to the breakthrough

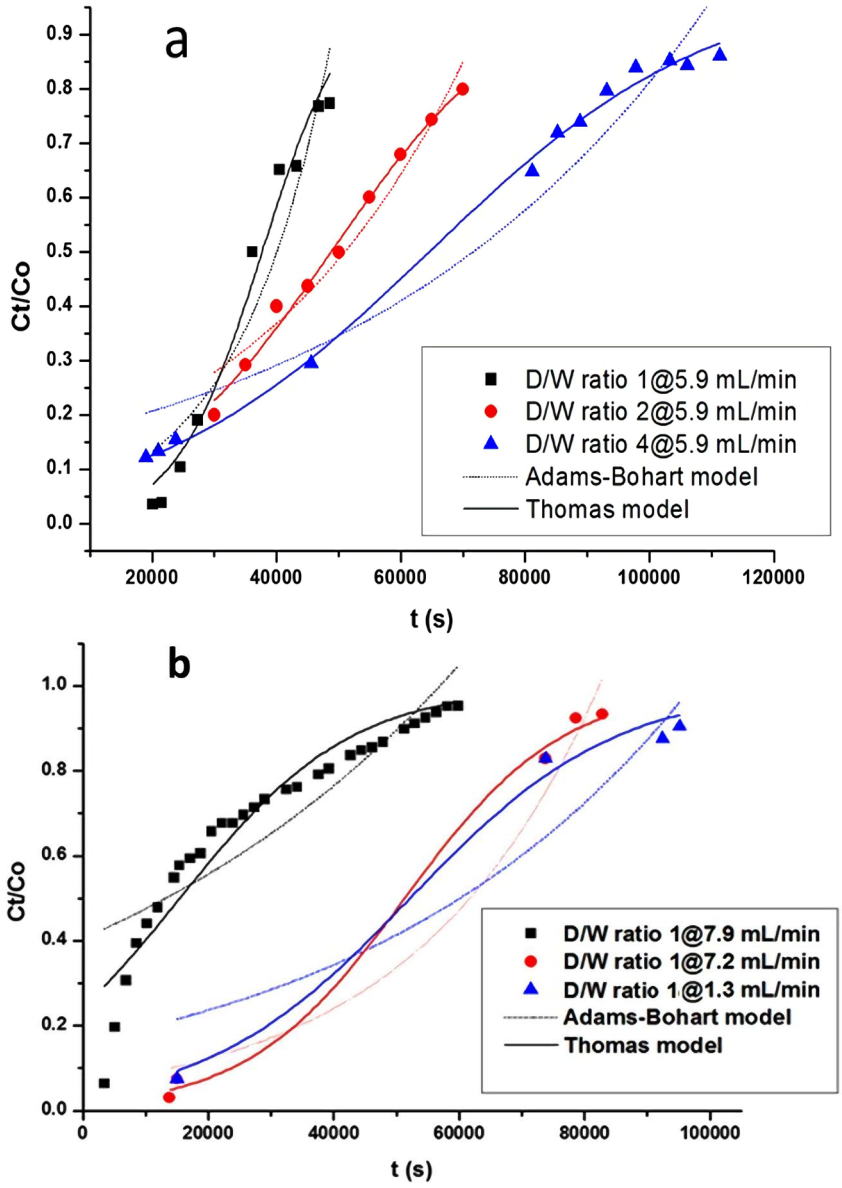

Figure 11. Breakthrough curves by the lab-scale IOCS column with variable parameters: (a) variable bed heights, and (b) variable flow rates.

experimental results, where the uranium adsorption capacity (q_e) was found to decrease as the flow rate decreased. This trend is consistent with the results reported by Nwabanne and Igbokwe (Nwabanne & Igbokwe, 2012). The following section used the non-linear method to fit the experimental data. Generally, the smaller value for SSE indicates a better fit of the model to the experimental data.

In Table 5 and Table 6, C_o is the initial influent concentration, H is the IOCS adsorbent media bed height, K_{ab} is the Adams-Bohart constant, K_{th} is the Thomas constant, N_o is the column adsorption capacity, Q is the flow rate, and SSE is the sum of squared errors. Comparing the SSE values between the non-linear fitted Adams-Bohart model in Table 5 and the non-linear fitting by the Thomas

Table 5. Adams-Bohart parameters at different conditions using the non-linear regression analysis.

C_o (kg·L^{-1})	Q (m^3·s^{-1})	H (m)	K_{ab} (L·kg^{-1}·s^{-1})	N_o (kg/L)	SSE
1.05E−06	9.83E−08	3.20E−02	6.26E+01	2.54E−04	7.24E−02
1.05E−06	9.83E−08	6.20E−02	2.65E+01	1.96E−04	1.39E−02
1.05E−06	9.83E−08	1.24E−01	1.63E+01	1.45E−04	6.15E−02
1.05E−06	2.17E−08	4.00E−02	1.78E+01	1.07E−04	5.77E−02
1.05E−06	1.20E−07	4.00E−02	3.20E+01	5.51E−04	2.01E−02
1.05E−06	1.32E−07	4.00E−02	1.51E+01	3.47E−04	3.18E−01

Table 6. Thomas parameters at different conditions using the non-linear regression analysis.

C_o (kg·L^{-1})	Q (m^3·s^{-1})	H (m)	K_{th} (L·kg^{-1}·s^{-1})	q_e (mg·kg^{-1})	SSE
1.05E−06	9.83E−08	3.20E−02	1.38E+02	1.30E+02	1.48E−02
1.05E−06	9.83E−08	6.20E−02	6.24E+01	8.78E+01	2.70E−03
1.05E−06	9.83E−08	1.24E−01	4.15E+01	5.81E+01	3.09E−03
1.05E−06	2.17E−08	4.00E−02	5.80E+01	3.96E+01	4.65E−03
1.05E−06	1.20E−07	4.00E−02	7.55E+01	2.37E+02	1.15E−01
1.05E−06	1.32E−07	4.00E−02	6.95E+01	6.49E+01	2.35E−03

model (Table 6), the smaller values of SSE obtained from the Thomas model indicates yield better prediction of the flow rate effects on the uranium adsorption process. The average Adams-Bohart constant in this case (Table 6) is 60.08 L·kg^{-1}·s^{-1}, while the average Thomas constant is 40.17 L·kg^{-1}·s^{-1}. The above discussed lab-scale data were utilized to optimize the operation parameters (flow rate, adsorbent bed height, and permeability of the IOCS bed) of the scaled-up filtration column.

Figure 12 shows the results of the lab-scale column tests that are based on the optimized operating conditions. The corresponding breakthrough curve indicates that some uranium appeared in the effluent on the 5th day of the test. In this optimized lab-scale test, approximately 40 g of mixed IOCS can immobilize uranium from the water at 1000 μg/L for 8 days at a flow rate of 0.28 mL/min in a 2.8 cm diameter column. This result serves as a baseline to compare with the field PRB test results.

3.9. Pilot Scale PRB Breakthrough Tests

The breakthrough curve obtained from the field test in Figure 13 showed a much earlier breakthrough threshold in comparison with the lab column test. The earlier breakthrough can be attributed to the shorter residence time or the presence of other anions in the influent during the field PRB test. The residence

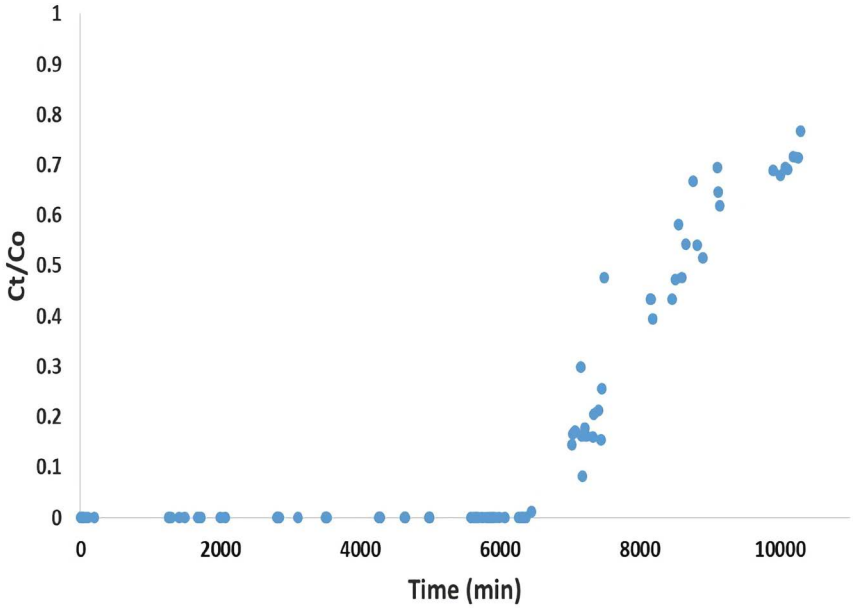

Figure 12. Lab-scale uranium removal in the fix-bed column at optimized conditions.

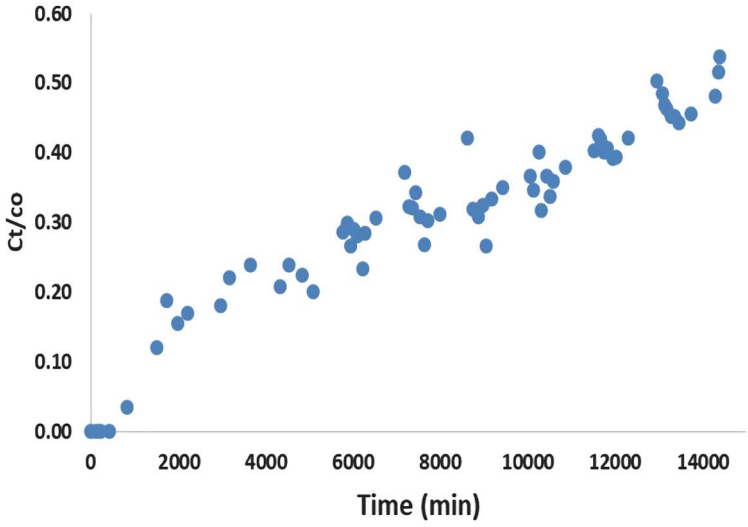

Figure 13. Uranium removal by the pilot PRB at the Gunnar pit site.

time is a crucial parameter to ensure adequate contact time between the IOCS media and the uranium containing water. To address this problem, a colored methylene blue dye could be used as a tracer to verify whether the designed 45 minute residence time was achieved or not. Another potential reason may relate to the presence of void spaces inside the IOCS bed. To reduce the air pocket formation during the sand loading process, filling of the PRB with water first and then adding IOCS adsorbents could help in packing the sand bed more effectively. Further optimization of the breakthrough experiment for the IOCS adsorbent would then be required. Parameters such as the water flow rate that contains uranium and various "depth-to-width" ratios of the IOCS bed should be further tested.

After the field test, the spent IOCS from different locations of the IOCS bed were collected for the uranium level analysis. Figure 14 shows the locations of the spent IOCS in the pilot-scale PRB that were sampled. These IOCS samples were sent to the SRC environmental analytical lab for uranium analysis. The amount of uranium in the spent IOCS at the end of the field test can help to determine whether the IOCS was effective in uranium removal. Figure 15 shows the uranium concentration in the IOCS sampled from different locations of the PRB box.

The average uranium concentration was 73 μg/kg in the bottom IOCS layer, 43 ppm in the middle layer, and 12 ppm uranium in the top layer. Since the pit water was pumped from the bottom to the top, the average uranium concentration in the IOCS increased from bottom to top. Some samples from the IOCS top layer showed higher uranium concentrations, which may be due to channeling within the IOCS adsorbent bed. These locations were close to the edges and corners of the pilot PRB where loosely packed IOCS media apparently allowed uranium containing water to bypass some portions of the IOCS bed. As a result, the IOCS bed was not uniformly utilized for uranium uptake from the uranium

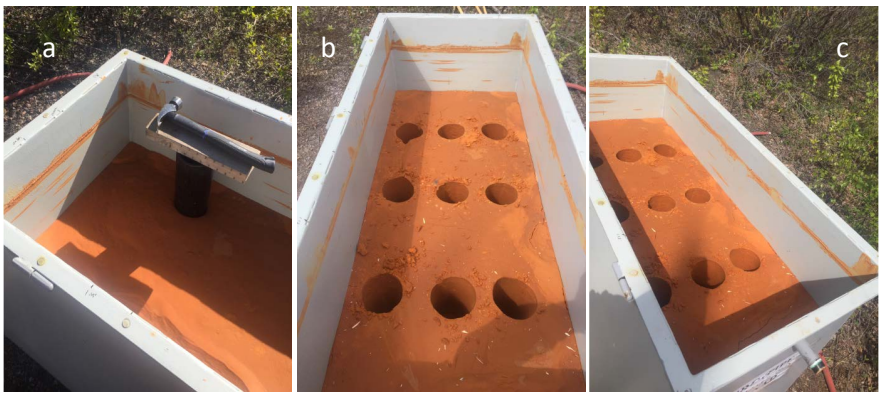

Figure 14. Spent IOCS sampling after the field test for uranium removal.

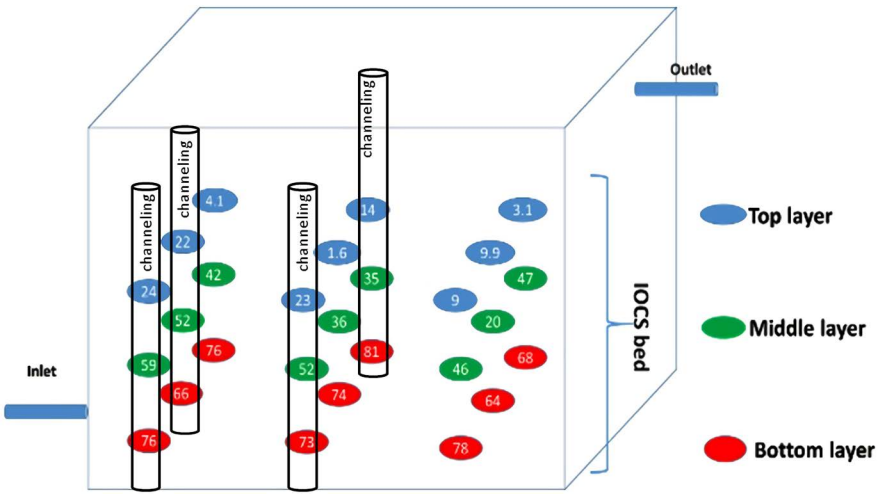

Figure 15. Uranium concentration (ppm) in the spent IOCS sampled from different locations inside the pilot PRB.

laden water. On the other hand, the uranium adsorption capacity of IOCS may also contribute to the performance of the field test results.

4. Conclusion

The IOCS media prepared herein was used to immobilize uranium species dissolved in the laboratory and environmental water samples. The lab test results showed the uranium removal capacity of IOCS is ca. 120 mg/kg at pH 7.3 under ambient operating conditions. Combining the lab batch adsorption test results and kinetic adsorption data, the lab-scale column tests were designed and performed to optimize the uranium removal process. The lab column test results showed that the breakthrough point is about 4.5 days, whereas the IOCS breakthrough occurred during the first day during field testing. The poor performance of the uranium immobilization observed in the field through the permeable reactive barrier is attributed here to insufficient residence time and the limited adsorption capacity of the IOCS adsorbent media.

Acknowledgements

The authors are grateful to the Saskatchewan Research Council and the University of Saskatchewan for supporting this research and the Innovation Fund support provided by the Government of Saskatchewan.

Conflicts of Interest

The authors declare no conflicts of interest regarding the publication of this paper.

References

Benjamin, M. M., Sletten, R. S., Bailey, R. P., & Bennett, T. (1996). Sorption and Filtration of Metals Using Iron-Oxide-Coated Sand. *Water Research, 30,* 2609-2620. https://doi.org/10.1016/S0043-1354(96)00161-3

Cornell, R. M., & Schwertmann, U. (2003). *The Iron Oxides: Structure, Properties, Reactions, Occurences and Uses.* Weinheim: Wiley-VCH GmbH& Co. KGaA. https://doi.org/10.1002/3527602097

Han, R. (2009). Adsorption of Methylene Blue by Phoenix Tree Leaf Powder in a Fixed-Bed Column: Experiments and Prediction of Breakthrough Curves. *Desalination, 245,* 284-297. https://doi.org/10.1016/j.desal.2008.07.013

Hubbe, M. A., Beck, K. R., O'Neal, W. G., & Sharma, Y. C. (2012). Cellulosic Substrates for Removal of Pollutants from Aqueous Systems: A Review. *BioResources, 9,* 5951-5962.

Jung, K. W., Kim, J. M., Kim, C. J., & Lee, J. M. (1987). Trace Analysis of Uranium in Aqueous Samples by Laser-Induced Fluorescence Spectroscopy. *Journal of the Korean Nuclear Society, 19,* 242-248.

Khan, M. N., & Sarwar, A. (2007). Determination of Point of Zero Charge of Natural and Treated Adsorbents. *Surface Review and Letters, 14,* 461-469. https://doi.org/10.1142/S0218625X07009517

Mahaninia, M., & Wilson, L. (2017). A Kinetic Uptake Study of Roxarsone Using Cross-Linked Chitosan. *Industrial & Engineering Chemistry Research, 56,* 1704-1712.

https://doi.org/10.1021/acs.iecr.6b04412

Markich, S. J. (2002). Uranium Speciation and Bioavailability in Aquatic Systems: An Overview. *The Scientific World Journal, 2,* 707-729. https://doi.org/10.1100/tsw.2002.130

Marshall, T. A., Morris, K., Law, G. T. W., Livens, F. R., Mosselmans, J. F. W., Bots, P., & Shaw, S. (2014). Incorporation of Uranium into Hematite during Crystallization from Ferrihydrite. *Environmental Science & Technology, 48,* 3724-3731. https://doi.org/10.1021/es500212a

Muldoon, J., & Schramm, L. L. (2009). Gunnar Uranium Mine Environmental Remediation—Northern Saskatchewan. In *the 12th International Conference on Environmental Remediation and Radioactive Waste Management* (pp. 1-12). Liverpool: ICEM2009. https://doi.org/10.1115/ICEM2009-16102

Muldoon, J., Yankovich, T., & Schramm, L. L. (2013). Gunnar Uranium Mine Environmental Remediation—Northern Saskatchewan. In *International Conference on Environmental Remediation and Radioactive Waste Management* (pp. 1-10). Brussels: ICEM2013. https://doi.org/10.1115/ICEM2013-96223

Nwabanne, J. T., & Igbokwe, P. K. (2012). Adsorption Performance of Packed Bed Column for the Removal of Lead (II) Using Oil Palm Fibers. *International Journal of Applied Science and Technology, 2,* 106-115.

Rusch, B., Hanna, K., & Humbert, B. (2010). Coating of Quartz Silica with Iron Oxides: Characterization and Surface Reactivity of Iron Coating Phases. *Colloids and Surfaces A: Physicochemical and Engineering Aspects, 353,* 172-180. https://doi.org/10.1016/j.colsurfa.2009.11.009

Schwertmann, U., & Cornell, R. M. (2000). *Iron Oxides in the Laboratory.* Chichester: Wiley. https://doi.org/10.1002/9783527613229

Sheng, L., & Fein, J. B. (2014). Uranium Reduction by *Shewanella oneidensis* MR-1 as a Function of $NaHCO_3$ Concentration: Surface Complexation Control of Reduction Kinetics. *Environmental Science & Technology, 48,* 3768-3775. https://doi.org/10.1021/es5003692

Sherman, D. M., Peacock, C. L., & Hubbard, C. G. (2008). Surface Complexation of U(VI) on Goethite (a-FeOOH). *Geochimica et Cosmochimica Acta, 72,* 298-310. https://doi.org/10.1016/j.gca.2007.10.023

Udoetok, I. A., Dimmick, R. M., Wilson, L. D., & Headley, J. V. (2016). Adsorption Properties of Cross-Linked Cellulose-Epichlorohydrin Polymers in Aqueous Solution. *Carbohydrate Polymers, 136,* 329-340. https://doi.org/10.1016/j.carbpol.2015.09.032

Xiong, W., & Peng, J. (2008). Development and Characterization of Ferrihydrite-Modified Diatomite as a Phosphorus Adsorbent. *Water Research, 42,* 4869-4877. https://doi.org/10.1016/j.watres.2008.09.030